2X-Thru De-Embedding Method Using Time Domain Impedance Response for S-Parameter Characterization of DUT in Broadband PCB

M. Seyedi, N. Masoumi**, P. Namaki, and S. Sheikhaei

School of Electrical and Computer Engineering, College of Engineering, University of Tehran, Tehran, Iran

Email: nmasoumi@ut.ac.ir

***Abstract*— This article introduces a unique application of the 2X-Thru de-embedding method, where it utilizes the impedance response of a structure—deviating from its conventional usage. The method is employed to mitigate the influence of Sub-Miniature version A (SMA) connectors in broadband printed circuit board (PCB) systems. For this purpose, two 50Ω microstrip lines are created on RO3003 laminates, accompanied by 1092-03A-6 edge-type 2.92mm female end launch connectors serving as error boxes on the designed transmission lines (test structures). To simulate these structures, the HFSS 3D electromagnetic (EM) simulator, renowned for its accuracy in real-world comparisons, is utilized. The method presents a sequential S-parameter model for the structure formed by the SMA connectors and the transmission lines. This enables discontinuous fixture S-parameter extraction up to 40 GHz. The precision of the method's extracted S-parameters is validated by comparing the obtained results from the microstrip line trace simulation with the outcomes of the de-embedding method applied to the test structures. The error between the de-embedded trace and the simulated one is minimal, measuring under 0.3 dB.**

Keywords— 2X-Thru, de-embedding method, SMA connector, printed circuit board (PCB), microstrip line, scattering

I. INTRODUCTION

To achieve accurate determination of the S-parameters of a Device Under Test (DUT) operating in the millimeter and sub-millimeter frequency ranges, de-embedding methods are employed. These methods serve to rectify the impact of passive structures and active circuits introduced by fixtures and interconnect parasitics [1]. The de-embedding process is essential to extract the intrinsic parameters of the DUT. De-embedding methods are categorized into three primary classifications, each defined by its distinct performance attributes: methods operating in the frequency domain, methods within the time domain, and methods that combine both frequency and time domains.

De-embedding methods in the frequency domain are classified into three principal categories, each delineated by its performance characteristics [2]: Cascaded Matrix Based Model (CMBM), Lumped Equivalent Circuit Model (LECM), and Cascaded Matrix with Lumped Equivalent Models (CMLEM).

CMBM category involves a meticulous separation of the effects attributed to fixtures and interconnect parasitics. Through mathematical operations performed on measurements from each distinct test structure, the characterization of the DUT is deduced. CMBM methods exhibit pronounced accuracy when dealing with expansive structures, where the maximum structure length (L_{max}) is greater than 0.1 times the wavelength (λ) [2]. Examples of methods in this category include the standard Thru-Reflect-Line (TRL) [3-6], Short-Open-Load-Thru (SOLT) [6, 7], and Line-Reflect-Match (LRM) [5, 6] de-embedding methods. However, implementing CMBM methods at the integrated circuit (IC) level can be costly due to space limitations [1].

LECM methods are well-suited for IC-level structures and are employed in wafer-level de-embedding [1]. LECM methods are simpler compared to other de-embedding methods and are particularly useful for low-frequency ranges. Illustrative methods within this classification encompass Open (O) and Open-Short (OS) [8-10] approaches.

CMLEM category encompasses more intricate methods capable of spanning a broader frequency spectrum. While CMLEM methods entail higher costs relative to LECM counterparts, they are adept at de-embedding DUTs with dimensions significantly smaller than the wavelengths of interest. Examples of CMLEM methods comprise L_iL_j [11] and the π-type L-2L de-embedding techniques [12-15].

The subsequent de-embedding category pertains to time domain methods; this classification is known as "time gating" [16]. Time-domain gating involves the precise delineation of a specific region within a temporal segment. The objective is to excise undesired responses, subsequently presenting the refined outcome in the frequency domain. Conceptually, gating can be envisioned as the multiplication of the time-domain response by a mathematical function, which takes on a value of one exclusively within the designated region of interest and remains at zero outside this interval. The gated time-domain function is then subject to a forward transformation, effectively rendering the frequency response while excluding the influence of other time domain responses [16].

The third category of de-embedding methods represents a convergence of two distinct realms: the time domain and the frequency domain. In these methods, the underlying principle involves leveraging the response characteristics, specifically the s-parameters, of de-embedding structures. These structures are designed to facilitate the extraction of the Device Under Test (DUT), which is the component or system of interest. In this approach, both the time domain and frequency domain aspects are integrated. The frequency domain element draws from the first category of de-embedding methods, where the focus lies in analyzing the response characteristics of signals at various frequencies. On the other hand, the time domain aspect borrows from the second category, which involves time-gating techniques to isolate relevant responses while excluding unwanted ones.

This specific classification of de-embedding methods was conceived with the primary objective of mitigating costs associated with the application of de-embedding techniques. The intention behind its formulation is to streamline the process by reducing the quantity of required de-embedding structures, consequently leading to a more economical implementation of de-embedding methods. The standard 2X-Thru [6] method and the approach outlined in [17] are encompassed within this classification.

The TRL method has been employed to set the reference plane to the measurement of inter-chip interconnect for heterogeneous millimeter-wave and THz Circuits [18], waveguide bandpass filter at D-band [19], and multiport micromachined waveguide interposer in sub-THz [20]. Although these methods have high accuracy, they need several fabricated standard structures for characterizing the fixtures, called calibration kits. TRL uses three standards, while 2X-Thru involves two sets of thru-line measurements. TRL can be complex but established, while 2X-Thru is simpler [21].

The 2X-Thru method includes automatic fixture removal (AFR) [22] and smart fixture de-embedding (SFD) [23] techniques. In [24], an error bound analysis is performed for both techniques. The method only needs a symmetrical Thru structure (calibration kit) to estimate the effects of fixtures and SMA connectors accurately. In this case, the de-embedding process can be accelerated and simplified by using scattering transfer parameters. In [25], the 2X-Thru method is introduced as a conventional de-embedding approach to address surface component effects in high-speed PCBs. The 2X-Thru de-embedding accuracy for uniform package transmission line devices under test (DUTs) is examined in [26]. The approaches of lX-Reflect SFD, 1-Port AFR, and 2X-Thru SFD compared across test fixture design, de-embedding procedures, and results in [27].

In the 2X-Thru de-embedding method, the time-domain channel characterization (TCC) is used to extract the S-parameters of the fixtures from the Thru structure. Design criteria of the symmetry pattern to avoid the error value of the de-embedding method result was proposed in [22] and also, analyzed the error sensitivity to estimate the error amplification after de-embedding in the TCC procedure. In [22] and [28], some techniques are proposed for de-embedding DUT using the TDR step response of the asymmetrical Thru structure. The frequency hybrid time domains method was proposed in [17] for de-embedding of asymmetric fixtures. However, the design process of the calibration kit to extract S-parameters of SMAs connectors is not illustrated in the previous approaches. Designing of calibration kit is very important for accurate operation of the 2X-Thru de-embedding method to extract S-parameters of DUT.

In this study, we fully describe the design process of the calibration kit for 2X-Thru de-embedding; then we propose an optimized Thru structure to de-embed any fixture and connector, employing 2X-Thru de-embedding. In this paper, we used the TDR impedance response to employ in the TCC algorithm. The TDR impedance response indicates discontinuity of structure much better than the TDR step response.

This paper is organized as follows: Section II introduces the designed structures for implementing the 2X-Thru method and elaborates on the utilization of transfer scattering parameters (T-parameters) within the de-embedding approach. Next the de-embedding methodology for the fixture S-parameters using 2X-Thru de-embedding method is thoroughly explained in Section III. Moreover, the accuracy of the de-embedded S-parameters of the microstrip line trace is examined by comparison with the simulated results. Finally, Section IV concludes the paper.

II. Designing Requaried Structures to Apply the 2x-Thru Method

Two structures for characterization of DUT are designed on two-layer HF RO3003 laminates. The DUT is connected to two SMAs with access line. The Sub-Miniature A (SMA) connector is an RF and microwave connector that is extensively used for indirect measurements, especially for RF connections within high-frequency (HF) electronic systems up to 40 GHz and sometimes more [29]. Usually, these connectors are main part of a fixture that is used to connect different measurement equipment to a DUT. These fixtures, especially SMA connectors add additional losses and reflections which degrade the performance of the DUT [29].

The structures consist of two SMA connectors with access line mounted on microstrip lines of different lengths as shown in Fig. 1(b) that represents two SMAs with their access line back-to-back connected (left and right fixture) with a short microstrip line trace (Thru structure). It's important to note that when extracting the specifications of the DUT, the chosen location (reference plain as shown in Fig.1) should be sufficiently distant from any discontinuities. Failure to do so could negatively impact the effectiveness of the de-embedding method's response. The microstrip line is 10mm long and 560um wide which leads to a characteristic impedance of 50Ω. Fig. 1(a) shows two SMAs with their access line back-to-back connected with a long microstrip line trace (Whole structure). In this case, the length of microstrip line trace is 100mm. These back-to-back connections of left fixture on one side of the microstrip line and right fixture on the other side make them possible to measure the DUT's S-parameters. The specifications of the PCB, most important for the design of transmission lines, are listed in Table 1.

TABLE I. The specifications of PCB

Specification	h_{die}	Width	tan δ	ε_{eff}
Value	$260\mu m$	$15mm$	0.0026	2.95

In a two-port network, conversion of S-parameters to T-parameters can be achieved using the formulas (1) and (2) [30].

$$T = \begin{bmatrix} \frac{1}{S_{21}} & \frac{-S_{22}}{S_{21}} \\ \frac{-S_{11}}{S_{21}} & \frac{S_{12}S_{21}-S_{11}S_{22}}{S_{21}} \end{bmatrix} \quad (1)$$

$$S = \begin{bmatrix} \frac{T_{21}}{T_{11}} & \frac{T_{11}T_{22}-T_{12}T_{21}}{T_{11}} \\ \frac{1}{T_{11}} & \frac{-T_{12}}{T_{11}} \end{bmatrix} \quad (2)$$

Using the cascaded T-matrices (chain transfer matrices) representation of the S-parameters for the designed structures

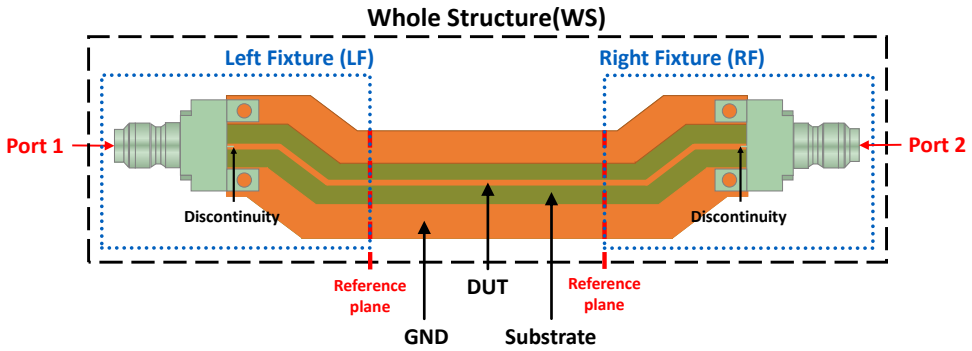

(a)

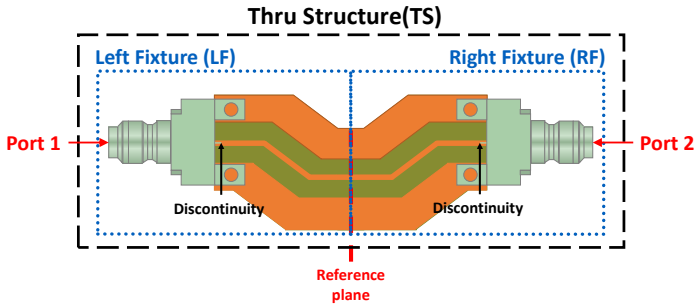

(b)

Fig. 1. Top view of the the designed structures for characterizing SMA connectors. (a) Whole structure (b) Thru structure.

yields the simple equations of (3) and (5) [31]. The left and right fixture S-parameters can be obtained from (3) using the 2X-Thru method, which will be described in the

next section. Equation (5) serves as the means to extract information from the Device Under Test (DUT), while also establishing the precision of the de-embedding method for the S-parameters of both extracted fixtures and the DUT. In this way, the de-embedded microstrip line trace is compared with the simulated microstrip line trace.

$$T_{TS} = T_{LF} * T_{RF} \tag{3}$$

$$T_{TS} = T_{LF} * T_{DUT} * T_{RF} \tag{4}$$

$$T_{DUT} = T_{LS}^{-1} * T_{WS} * T_{RS}^{-1} \tag{5}$$

where, the T_{TS} represents the chain transfer matrix of the Thru structures illustrated in Fig. 1(b), the T_{LF} and T_{RF} matrices represent the chain transfer matrix of the left and right fixture, the T_{WS} represents the chain transfer matrix of the Whole structures indicated in Fig. 1(a), and the T_{DUT} represents the chain transfer matrix of the intrinsic transmission-lines.

III. 2X-Thru De-embedding Method

A. De-embedding of Thru Structure in the Frequency Domain

To employ the AFR or SFD method, a Thru structure consisting of a 1x fixture and its mirror image needs to be designed [22]. A 1x fixture is an SMA connector with access line (left or right fixture) is connected to reference plane shown in Fig. 1. The S-parameters of the mirror image of the 1x fixture can be obtained by swapping Port 1 and Port 2 of the S-parameters of the 1x fixture. Since the left and right fixture (shown by LF and RF, respectively) are reciprocal and passive, their scattering parameters are mirror of each other. Assuming that the two fixtures have the same insertion losses, the equations (6), (7), and (8) are concluded [32].

$$S_{21}^{LF} = S_{12}^{LF} = S_{21}^{RF} = S_{12}^{RF} \tag{6}$$

$$S_{21}^{TS} = S_{12}^{TS} \tag{7}$$

$$S_{11}^{TS} = S_{22}^{TS} \tag{8}$$

Fig. 2 (a) and (b) indicate the Signal Flow Graph (SFG) of Whole and Thru structures, respectively. The SFG is a graphical representation that shows how waves propagate in an RF network. By applying Mason's four fundamental decomposition rules [32], the SFG of Thru structure (Fig.2 (b)) can be simplified into a single branch connecting two nodes, which makes it easier to achieve desired wave amplitude ratios [33]. From Mason's rules, the relations of the S-parameters of Thru structure and the two fixtures can be obtained. Equation (9) is derived from the SFG of Thru structure with four levels of simplification, as shown in Fig. 3.

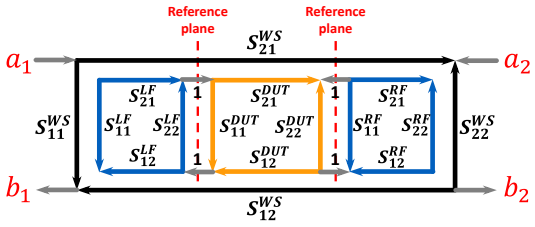

(a)

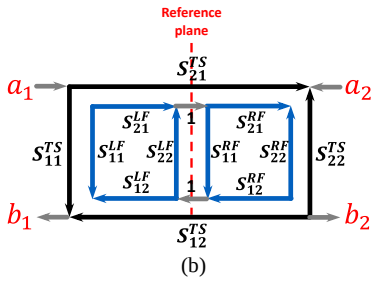

(b)

Fig. 2. The SFG of design structures. (a) Whole structure (b) Thru structure

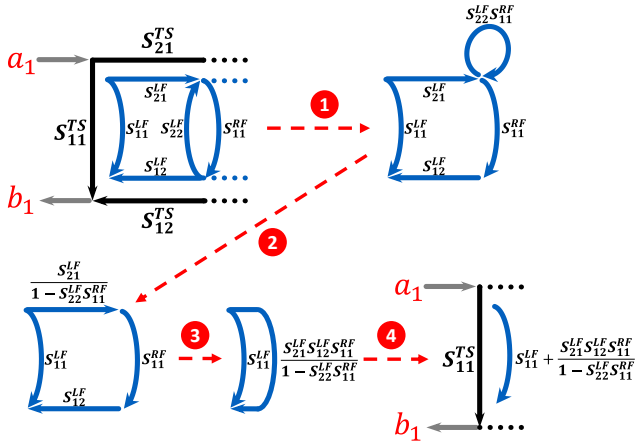

Fig. 3. The simplification of the SFG of Thru structure to obtain (9)

$$S_{11}^{TS} = S_{11}^{LF} + \frac{S_{11}^{RF} * S_{21}^{LF} * S_{12}^{LF}}{1 - S_{11}^{RF} * S_{22}^{LF}} \tag{9}$$

Furthermore, to obtain (10), the same method can be implemented from the other side of the SFG of the Thru structure.

$$S_{22}^{TS} = S_{22}^{RF} + \frac{S_{22}^{LF} * S_{21}^{BF} * S_{12}^{BF}}{1 - S_{11}^{RF} * S_{22}^{LF}} \tag{10}$$

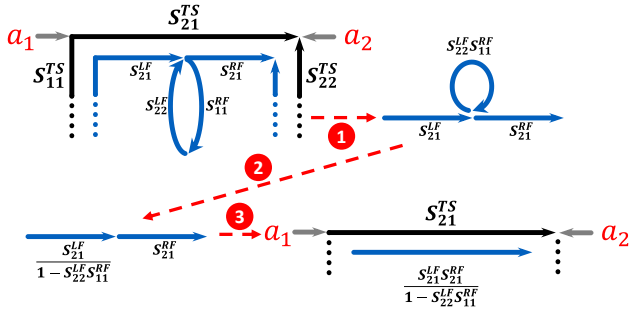

Fig. 4. The simplification of the SFG of Thru structure to obtain (11)

Equation (11) is a result of applying a sequence of three simplification stages to the SFG of the Thru structure, as depicted in Fig. 4.

$$S_{21}^{TS} = \frac{S_{21}^{LF} * S_{21}^{RF}}{1 - S_{11}^{RF} * S_{22}^{LF}} \tag{11}$$

Therefore, there are three unknown S-parameters left to be obtained. Accordingly, three equations are needed, while (9) and (10) represent a single equation, because it is reciprocal structure. In the following, time-domain reflectometry (TDR) is used to obtain the values of another unknown parameter.

In the above equations, S_{11}^{TS} and S_{21}^{TS} are acquired from the simulated Thru structures; S_{11}^{LF} is the S_{11} of the left fixture calculated from TDR response, thus we can have the S_{11} of the right-SMA or S_{11}^{RF} as follows:

$$S_{11}^{RF} = \frac{S_{11}^{TS} - S_{11}^{LF}}{S_{21}^{TS}} \tag{12}$$

Similarly, we also have:

$$S_{22}^{LF} = \frac{S_{22}^{TS} - S_{22}^{RF}}{S_{12}^{TS}} \tag{13}$$

After knowing S_{11}^{RF} and S_{22}^{LF}, from (12) and (13), we can conclude:

$$S_{21}^{LF} = \sqrt{S_{21}^{TS} * (1 - S_{11}^{RF} * S_{22}^{LF})} \tag{14}$$

B. Return Loss (S_{11}^{LF}) Extraction of SMA Connectors in Time Domain

The TDR response can be obtained from S_{11}^{TS}, using the IFFT [22, 24]. In our study, we obtained TDR response of Thru structure using HFSS simulator. The TDR impedance response generally consists of characteristics impedance of Thru structure in the time domain and indicates discontinuity, then demonstrates both mismatched areas along the whole channel. In order to solve two equations with three unknown variables, the TDR response is used as an additional method to provide one more equation. Equation (15) represents the relation of the characteristic impedance and the reflection ratio of the Thru structure.

$$Z_{2x}^{TDR} = 50\Omega \frac{1 + \Gamma_M^{2x}}{1 - \Gamma_M^{2x}} \tag{15}$$

Since the Thru structure includes the 1x-fixture (left fixture), the mirror image of the 1x-fixture (right fixture) and a short microstrip line trace between those is ideally symmetric by the middle point. The TDR impedance response (Z_{2x}^{TDR}) from the Thru structure has a time delay (T_d^{2x}). The T_d^{2x} is equal to two times of time delay from the left-SMA (T_d^{1x}) as shown in Fig. 2(a). Therefore, TDR response Z_{1x}^{TDR} of the fixture can be estimated by the modification of the TDR response of the Thru structure, as shown in Fig. 5(b). If the impedance at the middle point is 50Ω, the obtained reflection ratio is equal to the return loss S_{11}^{LF} while the reference impedance at the end of SMA in the Thru structure is not 50Ω. The obtained reflection ratio (Γ_M^{1x}) of the left fixture will be expressed in (16), with the actual reflection ratio (Γ_A) at the middle point [22]. The Γ_A occur when the characteristics impedance at the middle point is not 50Ω.

$$\Gamma_M^{1x} = S_{11}^{LF} + \frac{(S_{21}^{LF})^2}{\frac{1}{\Gamma_A} - S_{22}^{LF}} \tag{16}$$

Due to this fact, a 50Ω transmission line can be added to address the problem of obtaining the Γ_M^{1x}. As stated in [22], to calculate the return loss S_{11}^{LF} of the left fixture correctly, a very short transmission line is necessary between the fixtures, as shown in Fig. 1(b). This additional middle trace cannot be chosen very short. In other words, it should also be long enough to fulfill the time-domain channel characterization (TCC) algorithm.

With the aim of removing the estimated error in return loss S_{11}^{LF} of the left fixture in the Thru structure, the chosen length of the middle trace is 10mm based on (17) and (18) [22].

$$\left| \frac{S_{22}^{TS}}{S_{21}^{TS}} \right| < 1 \tag{17}$$

$$Length > \frac{v_c T_S}{2\sqrt{\varepsilon_{eff}}} \tag{18}$$

The waveform fluctuation caused by the first reflected wave on the TDR impedance response becomes stable after a specific time which is defined as timescale T_S ($T_S < 2T_d^{1x}$). In (18), v_c and ε_{eff} express the velocity of the light and the effective dielectric constant of PCB, respectively.

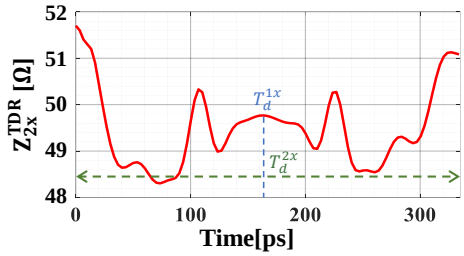

(a)

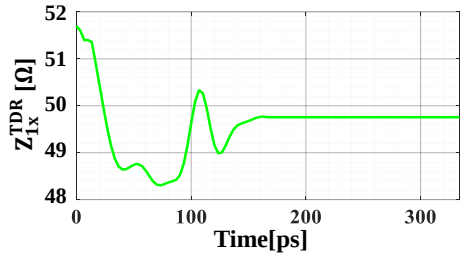

(b)

Fig. 5. TDR waveform of (a) Thru structure, (b) left-SMA

According to the above-mentioned conditions of TCC, we can estimate S_{11}^{LF} from S_{11}^{TS}. First, it is assumed that the left and the right port are terminated with a reference impedance. Based on the signal generation source, the incident waveform a_1 can be a stimulus signal, such as a delta function, a pulse function, or a step function. Using TDR response, we can obtain the reflected waveforms b_1 from (19).

$$\Gamma_M^{2x} = \frac{b_1}{a_1} = \frac{Z_{2x}^{TDR} - 50\Omega}{Z_{2x}^{TDR} + 50\Omega} \tag{19}$$

It is also assumed that the incident waveform is still a_1, at the left port of the left-SMA. The b_1' in (20) can be obtained by a middle time truncation and windowing the truncated time result [16] (Fig. 2(b)). The truncation of network frequency response data, which is similar to multiplying it with a rectangular window, has a mathematical equivalence. Subsequent inverse transformation of truncated data consistently yields a response featuring discernible "side lobes," especially if the original data does not approach zero before truncation. These side lobes can be prominent, potentially overshadowing the impedance response and prompting efforts for mitigation. A noteworthy outcome of truncation is the apparent non-causality of the response, evidenced by pre-zero side lobes in the impulse response. While not ideal, this is a mathematical reality. The side lobes in the truncated impedance response significantly elevate and persist, often obfuscating the intended function's response. Attenuating truncation's impact is most effective when the original function converges toward zero at the frequency endpoints. Employing a gradual windowing function allows for controlled attenuation of the frequency response, managing the emergence of side lobes arising from truncation.

$$\Gamma_M^{1x} = \frac{b_1'}{a_1} = \frac{Z_{1x}^{TDR} - 50\Omega}{Z_{1x}^{TDR} + 50\Omega} \tag{20}$$

Then, FFT is used to convert the time domain waveform to the frequency domain. Fourier analysis proves invaluable in representing physical responses and conducting network analyses. Nonetheless, practical measurements are inherently confined to acquiring finite frequencies within designated bandwidths. The FFT method requires 2^n data points, which the FFT distributes across the frequency range inversely to time spacing. Therefore, S_{11} of the left fixture in the frequency domain can be obtained as follows:

$$S_{11}^{LF} = \frac{fft\,(b_1')}{fft\,(a_1)} \tag{21}$$

Now the S-parameters of the two fixtures are known. Required data for the Thru structure (Fig. 1(a)), Whole structure (Fig. 1(b)), and single microstrip line trace are generated through the 3D full-wave electromagnetic (EM) simulations using the HFSS simulator. Fig. 8 depicts the de-embedded S-parameters of the microstrip line trace from the Whole structure, which is obtained from (5). The implementation steps for the 2X-Thru method are summarized and outlined in the flowchart depicted in Fig. 6.

The de-embedded S-parameters of the DUT exhibit accuracy of the method when placed together with the separately simulated S-parameters of the DUT. The maximum discrepancy of the de-embedded S-parameters of the DUT compared to the simulated one (see Fig. 7) is 0.3dB. Because of the limited number of simulation points in the time domain impedance response, the discrepancy has occurred.

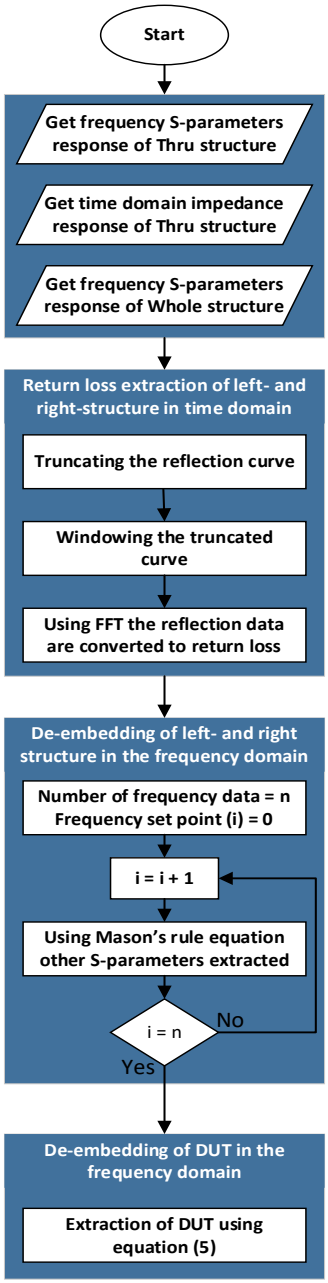

Fig. 6. Flowchart to depict the implementation steps of the 2X-Thru method.

Fig. 8 illustrates the de-embedded S-parameter results of the fixtures, spanning from DC to 40GHz. The amplitude of reflection loss ($|S_{11}|$) of the fixture increases from -55 to -18 dB and the amplitude of insertion loss ($|S_{21}|$) of the fixture decreases from 0 to -0.7 dB due to increasing the frequency from DC to 40 GHz, which is much less compared to the insertion loss of the 100mm microstrip line. Therefore, it can be concluded that the highest loss in the Whole structure is related to the microstrip line.

Fig. 7. Individually simulated structure of DUT

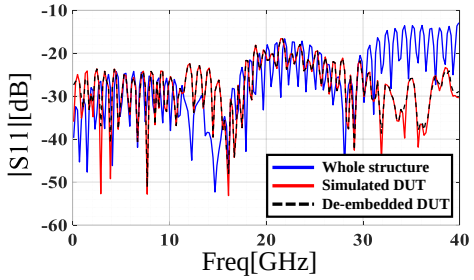

(a)

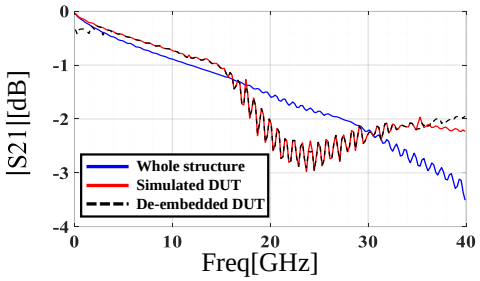

(b)

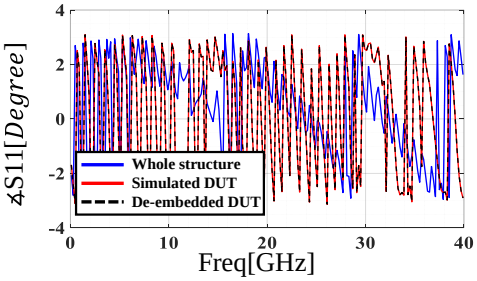

(c)

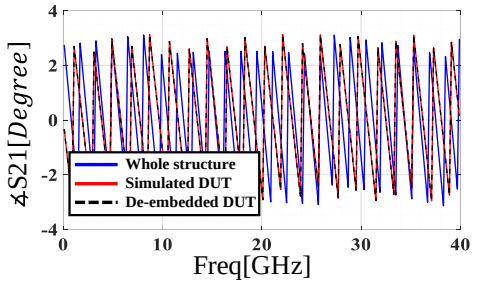

(d)

Fig. 8. S-parameters of de-embedded DUT compared to simulated trace. (a) amplitude of return loss, (b) amplitude of insertion loss, (c) phase of return loss, (d) phase of insertion loss.

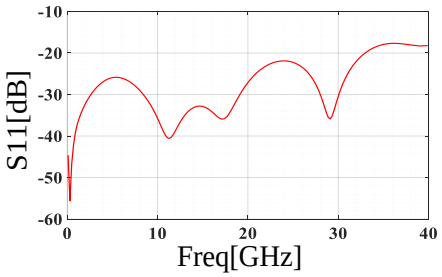

(a)

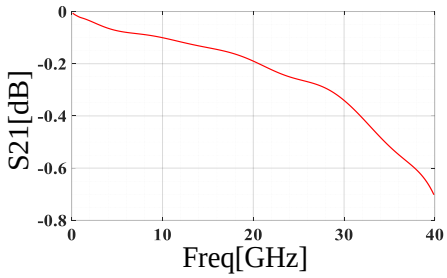

(b)

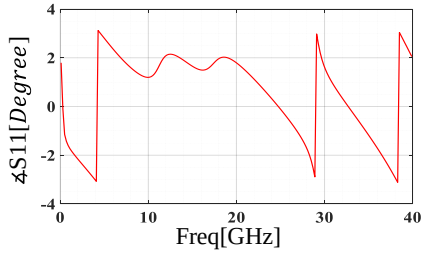

(c)

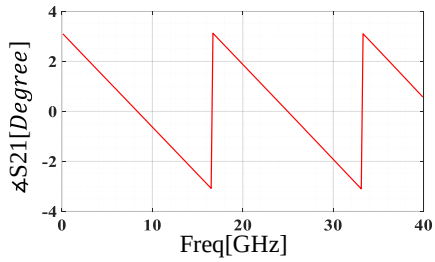

(d)

Fig. 9. S-pararmeters of de-embedded fixture. (a) amplitude of return loss, (b) amplitude of insertion loss, (c) phase of return loss, (d) phase of insertion loss.

IV. Conclusion

This paper introduces the use of the 2X-Thru de-embedding method to extract S-parameters from a microstripline, covering a frequency range up to 40GHz. A noteworthy aspect of this approach is its innovative application of impedance response, which presents a fresh perspective in methodology. The implementation was conducted using the HFSS 3D EM simulator and applied to simulation outcomes. To ensure accurate estimation of the microstripline's effects and those of the fixtures, the extraction process employs two distinct structures. Furthermore, the efficiency and simplicity of the de-embedding process are improved by employing scattering transfer parameters. An important highlight is the precision achieved in extracting the microstrip line trace (DUT), which showcases an error of less than 0.3dB when compared to the simulated trace. The results encompass evaluations of return loss and insertion loss for SMAs, along with their access line, over the entire frequency spectrum from DC to 40GHz.

V. Acknowledgment

The authors would like to thank the Circuits, Systems, and Test Laboratory (CST-Lab), School of Electrical and Computer Engineering, College of Eng., University of Tehran, researchers and technicians who provided insight, and comments that greatly assisted this paper.

References

[1] Lourandakis, Errikos. "On-Wafer Microwave Measurements and De-Embedding". Artech House, Norwood, 2016.

[2] Velayudhan, Vipin. “Vectorial measurement methods for millimeter wave integrated circuits.” (2016).

[3] K. Hoffmann and J. Raboch, "Hidden problems in precise calibration on microstrip II explanation and solution," 78th *ARFTG Microwave Measurement Conference*, 2011, pp. 1-5.

[4] L. Galatro, A. Pawlak, M. Schroter and M. Spirito, "Capacitively Loaded Inverted CPWs for Distributed TRL-Based De-Embedding at (Sub) mm-Waves," in *IEEE Transactions on Microwave Theory and Techniques*, vol. 65, no. 12, pp. 4914-4924, Dec. 2017.

[5] J. Stenarson and K. Yhland, "A Reformulation and Stability Study of TRL and LRM Using S -Parameters," in IEEE Transactions on Microwave Theory and Techniques, vol. 57, no. 11, pp. 2800-2807, Nov. 2009, doi: 10.1109/TMTT.2009.2032481.

[6] "IEEE Standard for Electrical Characterization of Printed Circuit Board and Related Interconnects at Frequencies up to 50 GHz," in IEEE Std 370-2020 , vol., no., pp.1-147, 8 Jan. 2021.

[7] R. A. Ginley, "Establishing traceability for SOLT calibration kits," 2017 *90th ARFTG Microwave Measurement Symposium (ARFTG)*, 2017, pp. 1-4.

[8] B. Zhang, Y.-Z. Xiong, L. Wang, S. Hu, and J. L.-W. Li, “On the De-Embedding Issue of Millimeter Wave and Sub-Millimeter-Wave Measurement and Circuit Design,” IEEE Trans. Compon. Packag. Manuf. Technol., vol. 2, no. 8, pp. 1361–1369, Aug. 2012.

[9] T. E. Kolding, “A Four-Step Method for De-Embedding Gigahertz On-Wafer CMOS Measurements,” IEEE Trans. Electron Devices, vol. 47, no. 4, pp. 734–740, Apr. 2000.

[10] A. Hamidipour, M. Jahn, F. Starzer, X. Wang, and A. Stelzer, “On-Wafer Passives De-Embedding Based on Open-Pad and Transmission Line Measurement,” in 2010 IEEE Bipolar/BiCMOS Circuits and Technology Meeting (BCTM), pp. 102–105, 2010.

[11] N. Erickson, K. Shringarpure, J. Fan, B. Achkir, S. Pan and C. Hwang, "De-embedding techniques for transmission lines: An exploration, review, and proposal," 2013 IEEE International Symposium on Electromagnetic Compatibility, 2013, pp. 840-845.

[12] H. -Y. Cho, J. -K. Huang, C. -W. Kuo, S. Liu and C. -Y. Wu, "A Novel Transmission-Line Deembedding Technique for RF Device Characterization," in IEEE Transactions on Electron Devices, vol. 56, no. 12, pp. 3160-3167, Dec. 2009.

[13] N. Erickson, B. Achkir and J. Fan, "Revised L–2L Method for On-Chip De-Embedding," in IEEE Transactions on Electromagnetic Compatibility, vol. 61, no. 1, pp. 209-216, Feb. 2019.

[14] S. Kawai, K. K. Tokgoz, K. Okada and A. Matsuzawa, "L-2L de-embedding method with double-T-type PAD model for millimeter-wave amplifier design," 2015 IEEE 15th Topical Meeting on Silicon Monolithic Integrated Circuits in RF Systems, San Diego, CA, USA, 2015, pp. 43-45.

[15] N. Li, K. Matsushita, N. Takayama, S. Ito, K. Okada, and A. Matsuzawa, “Evaluation of a multi-line de-embedding technique up to 110 GHz for millimeter-wave CMOS circuit design,” IEICE Trans. Fundamentals Electron., Commun. Comput. Sci., vol. E93-A, no. 2, pp. 431–439, Feb. 2010.

[16] Dunsmore, Joel, P. Handbook of microwave component measurements with advanced VNA techniques. John Wiley & Sons, 2020.

[17] Yao, S., Wei, X. -C. & Ding, L. A Deembedding Method for the S-Parameter Extraction of Surface-Mounted Devices With Asymmetric Fixtures, in IEEE Microwave and Wireless Components Letters, vol. 31, no. 2, pp. 211-214 (2021). doi: 10.1109/LMWC.2020.3034124.

[18] Fay, P., Bernstein, G.H., Lu, T. *et al*. Ultra-wide Bandwidth Inter-Chip Interconnects for Heterogeneous Millimeter-Wave and THz Circuits. *J Infrared Milli Terahz Waves* 37, 874–880 (2016). https://doi.org/10.1007/s10762-016-0278-5.

[19] Vazquez-Roy, J.L., Rajo-Iglesias, E., Ulisse, G. et al. Design and Realization of a Band Pass Filter at D-band Using Gap Waveguide Technology. J Infrared Milli Terahz Waves 41, 1469–1477 (2020). https://doi.org/10.1007/s10762-020-00729-8.

[20] Gomez-Torrent, A., Oberhammer, J. Micromachined Waveguide Interposer for the Characterization of Multi-port Sub-THz Devices. J

Infrared Milli Terahz Waves 41, 245–257 (2020). https://doi.org/10.1007/s10762-019-00663-4.

[21] S. -J. Moon, X. Ye and R. Smith, "Comparison of TRL calibration vs. 2x thru de-embedding methods," 2015 IEEE Symposium on Electromagnetic Compatibility and Signal Integrity, Santa Clara, CA, USA, 2015, pp. 176-180, doi: 10.1109/EMCSI.2015.7107681.

[22] C. Yoon et al. Design Criteria and Error Sensitivity of Time-Domain Channel Characterization (TCC) for Asymmetry Fixture De-Embedding, in IEEE Transactions on Electromagnetic Compatibility, vol. 57, no. 4, pp. 836-846 (2015). doi: 10.1109/TEMC.2014.2379627.

[23] Wu, C., Chen, B., Mikheil, T., Fan, J. & Ye, X. Error bounds analysis of de-embedded results in 2x thru de-embedding methods, 2017 IEEE International Symposium on Electromagnetic Compatibility & Signal/Power Integrity (EMCSI), pp. 532-536 (2017). doi: 10.1109/ISEMC.2017.8077927.

[24] C. Wu, B. Chen, T. Mikheil, J. Fan and X. Ye, "Error bounds analysis of de-embedded results in 2x thru de-embedding methods," 2017 IEEE International Symposium on Electromagnetic Compatibility & Signal/Power Integrity (EMCSI), Washington, DC, USA, 2017, pp. 532-536, doi: 10.1109/ISEMC.2017.8077927.

[25] J. -Y. Ye, J. Fan, X. Cao, Q. -M. Cai, Y. Zhu and Y. Zhu, "A 2x-Thru Standard De-embedding Method of Surface Components in High-Speed PCBs," 2022 IEEE USNC-URSI Radio Science Meeting (Joint with AP-S Symposium), Denver, CO, USA, 2022, pp. 58-59, doi: 10.23919/USNC-URSI52669.2022.9887402.

[26] S. A. Smith, Z. Zhang and K. Aygün, "Assessment of 2x Thru De-embedding Accuracy for Package Transmission Line DUTs," 2020 IEEE 29th Conference on Electrical Performance of Electronic Packaging and Systems (EPEPS), San Jose, CA, USA, 2020, pp. 1-3, doi: 10.1109/EPEPS48591.2020.9231405.

[27] Y. Chen, B. Chen, J. He, R. Zai, J. Fan and J. Drewniak, "De-embedding comparisons of 1X-Reflect SFD, 1-port AFR, and 2X-Thru SFD," 2018 IEEE International Symposium on Electromagnetic Compatibility and 2018 IEEE Asia-Pacific Symposium on Electromagnetic Compatibility (EMC/APEMC), Suntec City, Singapore, 2018, pp. 160-164, doi: 10.1109/ISEMC.2018.8393759.

[28] Barnes, H. & Moreira, J. Verifying the accuracy of 2x-Thru de-embedding for unsymmetrical test fixtures, 2017 IEEE 26th Conference on Electrical Performance of Electronic Packaging and Systems (EPEPS), pp. 1-3 (2017). doi: 10.1109/EPEPS.2017.8329760.

[29] Jesch, R. L. (1976) Repeatability of SMA coaxial connectors, in IEEE Transactions on Instrumentation and Measurement, vol. IM-25, no. 4, pp. 314-320, doi: 10.1109/TIM.1976.6312234.

[30] Frickey, D. A. Conversions between S, Z, Y, H, ABCD, and T parameters which are valid for complex source and load impedances, in IEEE Transactions on Microwave Theory and Techniques, vol. 42, no. 2, pp. 205-211 (1994). doi: 10.1109/22.275248.

[31] Adamian, V. and Cole, B. A novel procedure for characterization of multiport high-speed balanced devices, 2006 IEEE International Symposium on Electromagnetic Compatibility, 2006. EMC. pp. 395-398 (2006). doi: 10.1109/ISEMC.2006.1706334.

[32] Pozar, David, M. Microwave engineering. John Wiley & Sons, 2009.

[33] Mason, S. Feedback theory-some properties of signal flow graphs, Proc. IRE, vol. 41, no. 9, pp. 1144–1156, (1953).